03,12

The effect of introducing monoethanolammonium cation into hybrid halide perovskite films on the nature of their low-temperature conductivity

© M.K. Ovezov[1], A.A. Ryabko[1], P.A. Aleshin[1], A.N. Lodygin[1], I.A. Vrublevskiy[2], V.A. Moshnikov[3], A.N. Aleshin[1]

[1] Ioffe Institute,
St. Petersburg, Russia
[2] Belarusian State University of Informatics and Radioelectronics,
Minsk, Belarus
[3] St. Petersburg State Electrotechnical University „LETI"
St. Petersburg, Russia

E-mail: strontiumx94@gmail.com

Received July 2, 2025
Revised July 2, 2025
Accepted July 3, 2025

Hybrid organo-inorganic halide perovskites are promising materials for optoelectronic devices. In this work, it was shown that the introduction of the monoethanolammonium cation MEA into the hybrid perovskite $MAPbI_3$ leads to a change in the characteristic absorption peaks of FTIR spectroscopy, indicating chemical interaction of the monoethanolammonium cation with the hybrid perovskite. An increase in the proportion of the monoethanolammonium cation in the hybrid perovskite leads to an increase in the absorption edge energy of the perovskite and a significant change in the shape of the spectra, as well as to a change in the band diagram. Low-temperature conductivity (in the range of 100−200 K) is characterized by suppression of the ionic component, which is also accompanied by a significant decrease in the hysteresis of the current-voltage characteristics of the films. The results of measuring the temperature dependence of the current-voltage characteristics showed that the use of the monoethanolammonium cation in the hybrid perovskite leads to an increase in the activation energy of ionic conductivity and a decrease in hysteresis, which helps to reduce the degradation of devices based on hybrid perovskites.

Keywords: hybrid halide perovskites, monoethanolammonium cations, solar cells, low-temperature conductivity, hysteresis, I-V characteristics.

DOI: 10.61011/PSS.2025.08.62252.174-25

1. Introduction

Hybrid halide perovskites are regarded today as the most promising materials for use in new-generation solar cells [1–3]. It is due to a high light absorption coefficient, a large free path length of charge carriers and an adjustable band gap [4]. These materials are also interesting for use in photodetectors and X-ray detectors as well as in memristor structures [5–7].

As of today, the hybrid halide perovskites $APbX_3$ to be applied in the solar cells usually include organic cations (A) of methylammonium (MA^+) and formamidinium (FA^+) with addition of a small portion of inorganic cations Cs^+, Rb^+, and I^- ions with addition of Br^- or Cl^- ions as anions (X). Perovskites with replacement of atoms of the metal Sb with Sn are widely studied [8]. The different cations and anions are used simultaneously due to adjustment of the band gap and a position of the energy levels, but also due to increase of chemical stability, increase of ion migration activation energy for reducing degradation of devices in an operating mode [8–11]. Ion migration is also reduced by using molecular passivation on grain boundaries and, additionally, 2D-layer hybrid perovskites [12,13], which are characterized by reduced ion migration, and higher chemical stability, higher resistivity and the larger band gap [14]. Thus, using a wide class of amines for molecular passivation of the grain boundaries of the polycrystalline layers or for formation of the 2D-layer perovskites for their inclusion in a photovoltaic structure is one of the main trends in the field of investigation of the hybrid perovskites for improving stability of their parameters and preserving high efficiency of perovskite solar cells.

The present study has investigated hybrid halide perovskites with addition of a monoethanolammonium cation ($HOCH_2CH_2NH_3^+$, MEA^+), namely, perovskites using the cation of methylammonium and monoethanolammonium $MA_xMEA_{1-x}PbI_3$. The MEA^+ cation is characterized by presence of OH groups. It was noted in the study [15], in which the 2D perovskite $HO(CH_2)_2NH_3)_2PbX_4$ was synthesized using the monoethanolammonium cation, that presence of the OH groups resulted in formation of intermolecular hydrogen bonds with $NH_3^+ \cdots OH$. Dipoles induced by the hydroxyl group result in increase of relative permittivity, thereby decreasing the exciton's bond energy

and increasing charge separation efficiency [16]. It is assumed that using the MEA^+ cation included in a bulk ($3D$) perovskite results in formation of channels in the crystalline structure [17,18]. As a whole, data of X-ray diffraction analysis indicate that interplanar spacings of the crystal lattice of the tetragonal phase of the perovskite increase with increase of the MEA^+ portion, which also correlates with increase of the band gap [17,19]. The increase of the MEA^+ portion and the band gap of $MA_xMEA_{1-x}PbI_3$ makes it a promising material for application in tandem solar cells with silicon structures [19,20]. A small MEA^+ portion included in the hybrid perovskite can increase stability of its parameters. Thus, in the study [21] the solar cell based on the hybrid perovskite $MAPbI_3$ with addition of MEA^+ demonstrated increased stability in the operating mode. Thus, the hybrid perovskites $MA_xMEA_{1-x}PbI_3$ are of considerable interest, but still understudied.

The present study was aimed at investigating the influence of the MEA portion in the hybrid perovskite $MA_xMEA_{1-x}PbI_3$ on temperature dependences of I-V characteristics and resistivity within the temperature range 300−100 K. The dependence of the I-V characteristics on the temperature makes it possible to record a decrease of hysteresis due to an ion component of conductivity and to determine an energy of activation of ion conductivity in the polycrystalline layer of the hybrid perovskite. Due to correlation of the ion component of conductivity (mobile defects) in the hybrid perovskites with performance of devices (the solar cells of the photoresistors), namely, with degradation of their characteristics in the operating mode, determination of the energy of activation of ion conductivity is one of the most important characteristics of a material based on the hybrid perovskite [22].

2. Materials and methods

The monoethanolammonium iodide (MEAI, $HOCH_2CH_2NH_3I$) was produced by neutralizing monoethanolamine ($HOCH_2CH_2NH_2$, JSC „LenReaktiv“, Saint-Petersburg, Russia) with hydrogen iodide acid (HI, JSC „LenReaktiv“, Saint-Petersburg, Russia) until obtaining $pH = 6.5$. After that, the solution was vaporized at 90 °C in a water bath and a produced precipitate was filtered in vacuum. MEAI and lead iodide (PbI_2, Xi'an Yuri Solar Co., Ltd., Xi'an, China) was separately dissolved in dimethylformamide (DMFA, C_3H_7NO, JSC „LenReaktiv“, Saint-Petersburg, Russia). The two produced solutions were mixed in a molar ratio 1:1, with keeping the constant temperature of 60 °C during the process. Similarly, methylammonium iodide (MAI, CH_3NH_3I, Xi'an Yuri Solar Co., Ltd., Xi'an, China) and PbI_2 that were dissolved in DMFA were mixed in the molar ratio 1:1 at 60 °C (in order to produce $MAPbI_3$, $CH_3NH_3PbI_3$).

By mixing the produced solutions of MAI-PbI_2 and MEAI-PbI_2 in the ratios 1:1, 3:1 and 1:3, initial solutions were prepared in order to produced the hybrid perovskites with the general formula $MA_xMEA_{1-x}PbI_3$ ($MA_{0.75}MEA_{0.25}PbI_3$, $MA_{0.5}MEA_{0.5}PbI_3$ and $MA_{0.25}MEA_{0.75}PbI_3$). The polycrystalline films are produced by crystallization of the perovskite phase when heating the solutions, which is accompanied by evaporation of organic solvents. The polycrystalline layers $MA_xMEA_{1-x}PbI_3$ were produced by centrifugation from the DMFA and dimethylsulfoxide solution (DMSO, C_2H_6OS, JSC „LenReaktiv“, Saint-Petersburg, Russia) in a volume ratio 4:1. The concentration of $MA_xMEA_{1-x}PbI_3$ in the DMFA and DMSO solution was 400 mg/ml. The process included a stage of pre-centrifugation at the speed of 1000 rpm (for 10 seconds) and centrifugation at the speed of 3000 rpm (for 30 seconds) to produce a thin film of the solution. Then the samples were placed on a heating plate designed to control and stabilize the temperature (WiseTherm HP-20D) with the temperature of 110 °C for a crystallization process with formation of solid polycrystalline layers of $MA_xMEA_{1-x}PbI_3$ for 10 minutes. In order to measure the absorption spectra (the spectrophotometer SPEKS SSP−715, JSC „SPEKS“, Moscow, Russia), the polycrystalline layers were applied to glass substrates. The perovskite films were also studied by means of the Fourier transform infrared spectroscopy using the spectrometer FSM 2201 (LLC „Infraspec“, Saint-Petersburg, Russia). For this purpose, the layers were applied to plates made of single crystal silicon grown by zone melting. In order to measure the I-V characteristics (IVC), the $MA_xMEA_{1-x}PbI_3$ films were applied to ceramic substrates golden interdigital electrodes (Sensor Platform, Tesla Blatna, a.s., Blatna, Czech Republic). An Au-strip width of the interdigital electrodes and a distance between them were 25 μm, while the total electrode area was 4.2×4.2 mm. The I-V characteristics of the films that were placed on a holder of the optical continuous-flow cryostat with temperature stabilization OPTCRYO198 (JSC „RTI“, Moscow, Russia) were measured in a nitrogen atmosphere in darkness at the temperature 100−300 K using an automated measurement installation based on a pico-ammeter Keithley 6487 (Keithley Instruments, Solon, USA).

3. Results and discussion

The results of the Fourier transform infrared spectroscopy of transmittance of the $MA_xMEA_{1-x}PbI_3$ films within the range 400−4000 cm^{-1} are shown in Figure 1, where the lines mark the most intense absorption bands of $MAPbI_3$. The spectrum for $MAPbI_3$ was analyzed based on the study [23], which provides results of simulation of vibrational modes for the hybrid perovskite $MAPbI_3$ within the range from 0 to 3100 cm^{-1} for the infrared and Raman-scattering spectroscopy as well as compares theoretical results and experimental results of the IR spectroscopy at the temperature 295 and 10 K.

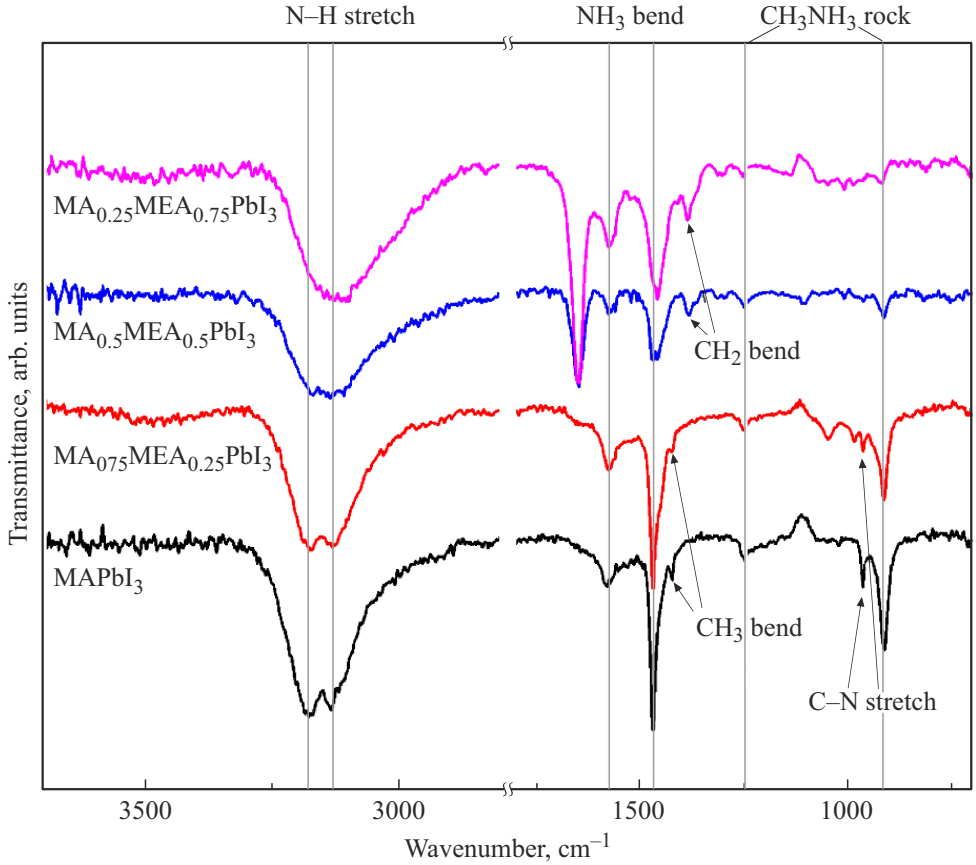


Figure 1. Fourier transform infrared spectroscopy of the hybrid perovskites $MA_xMEA_{1-x}PbI_3$.

As can be seen in Figure 1, at the frequencies 3177 and 3132 cm^{-1} the IR Fourier spectrum $MAPbI_3$ exhibits valence (stretching) N-H oscillations (νN-H) due to NH_3^+ groups that also determine strain (bending) oscillations at the frequencies 1580 and 1470 cm^{-1} (δNH_3). The increase of the portion of the monoethanolammonium cation in $MA_xMEA_{1-x}PbI_3$ results in a slight shift of the frequency of the νN-H oscillations, which can be related not only to variation of the parameters of the crystal lattice in $MA_xMEA_{1-x}PbI_3$, but to formation of the hydrogen bonds $NH_3^+ \cdots OH$. For the hybrid perovskites $MA_{0.5}MEA_{0.5}PbI_3$ and $MA_{0.25}MEA_{0.75}PbI_3$, separate oscillations νN-H become indistinguishable. At the same time, no noticeable shift of the frequency for the δNH_3 oscillations is observed, but one can notice a slight change of intensity of δNH_3 at the frequency of 1470 cm^{-1} relative to a band at the frequency of 1580 cm^{-1}. The νC-N stretching is observed for $MAPbI_3$ and $MA_{0.75}MEA_{0.25}PbI_3$, but it is not recorded already for $MA_{0.5}MEA_{0.5}PbI_3$ and $MA_{0.25}MEA_{0.75}PbI_3$.

Generally, the spectra of $MAPbI_3$ and $MA_{0.75}MEA_{0.25}PbI_3$ differ slightly. The spectra for $MAPbI_3$ and $MA_{0.75}MEA_{0.25}PbI_3$ exhibit absorption bands related to strain pendulum (rocking) oscillations of δCH_3NH_3 as well as slight absorption bands related to δCH_3 oscillations, which are not recorded for the compositions $MA_{0.5}MEA_{0.5}PbI_3$ and $MA_{0.25}MEA_{0.75}PbI_3$ except for the most intensive absorption band of δCH_3NH_3 at the frequency of 910 cm^{-1}. The spectra of $MA_{0.5}MEA_{0.5}PbI_3$ and $MA_{0.25}MEA_{0.75}PbI_3$ do not exhibit typical bands of absorption of pure monoethanolamine, which also confirms incorporation of the MEA^+ cations into the crystal lattice of the hybrid perovskite jcite24. With the increase of the MEA^+ portion (in the spectra of $MA_{0.5}MEA_{0.5}PbI_3$ and $MA_{0.25}MEA_{0.75}PbI_3$), instead of the δCH_3 absorption band there is an absorption band at the frequency $\sim$ 1380 cm^{-1}, which can be related to the δCH_2 oscillations. Finally, the transmittance spectra of $MA_{0.5}MEA_{0.5}PbI_3$ and $MA_{0.25}MEA_{0.75}PbI_3$ exhibit an intense absorption band at the frequency $\sim$ 1650 cm^{-1}, which can be caused by oscillations of the hydrogen bonds $NH_3^+ \cdots OH$ [26].

The increase of the portion of the monoethanolammonium cation in the hybrid perovskite $MA_xMEA_{1-x}PbI_3$ results both in the shift of an absorption edge and in a change of the absorption spectrum shape (Figure 2). When the MEA^+ portion is 25 %, the shift of the absorption edge and, respectively, the increase of the optical band gap is insignificant. Besides, there are similar inflection points that are typical for the hybrid perovskite $MAPbI_3$. According to the study [27], in this energy range the absorption range of $MAPbI_3$ is mainly determined by interband transitions between a ceiling of the valence band (the energy-highest valence band VB_1) and a bottom of the conduction band

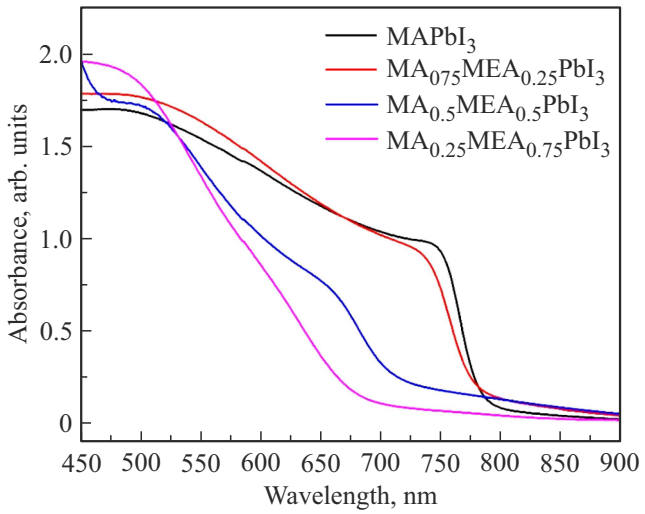


Figure 2. Spectra of absorbance of the films of the hybrid perovskite $MA_xMEA_{1-x}PbI_3$, which are formed by centrifugation on the glass substrates.

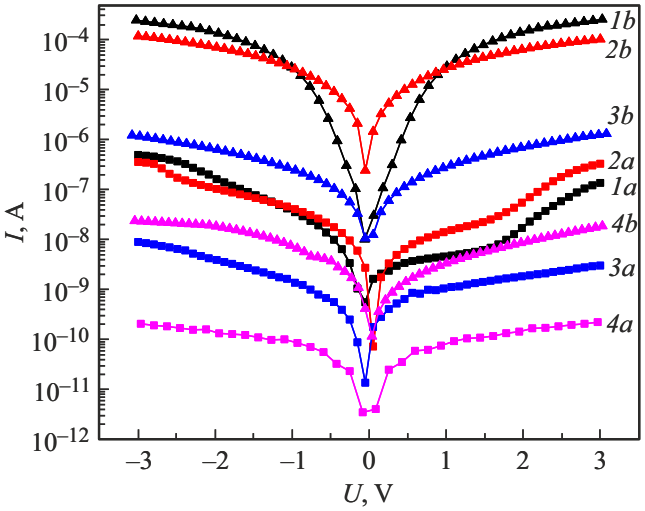


Figure 3. I-V characteristics of the films of the hybrid perovskites $MA_xMEA_{1-x}PbI_3$ in darkness (*a*) and at irradiation (*b*). *1* — $x = 0$; *2* — $x = 0.25$; *3* — $x = 0.5$; *4* — $x = 0.75$.

(the energy-lowest conduction band CB_1). With more details, starting from the energy ~ 1.6 eV, absorption is caused by the interband transitions VB_1-CB_1 in the symmetry point R in the first Brillouin zone, while starting from the energy ~ 2.5 eV, it is caused by VB_1-CB_1 in the symmetry point M with a slight contribution by the VB_1-CB_2 (the energy-second conduction band) in the point R.

The preserved spectrum shape for $MA_{0.75}MEA_{0.25}PbI_3$ indicates a slight change of the energy band diagram. In this energy range, the absorption spectrum of $MA_{0.5}MEA_{0.5}PbI_3$ exhibits similar inflection points that are probably related to two kinds of the interband transitions VB_1-CB_1 in the symmetry points R and M, as well as the shift of the absorption edge. However, the first peak caused by the transitions VB_1-CB_1 in the symmetry point R is somewhat smoothened. Finally, for $MA_{0.25}MEA_{0.75}PbI_3$ the peak due to VB_1-CB_1 in the point R becomes insignificant, which is untypical for the absorption spectra of the hybrid perovskites, including wider-band ones. It can be assumed in the model of the crystalline structure of the perovskites with channels, where the band gap is increased due to violation of binding of PbI_6 octahedrons, as described in the study [17], that the change of the absorption spectra shape can be related to some dispersion of the bound octahedrons, which results in „smearing“ of the peak.

All the polycrystalline $MA_xMEA_{1-x}PbI_3$ films that are applied to the ceramic substrates with the interdigital Au electrodes, demonstrate a significant photoresponse when being irradiated by a solar radiation simulator (Figure 3) that provides specific radiation power of $1\,kW/m^2$.

A thickness of the films on the ceramic substrates can be different due to different solution wettability, conditions of solvent evaporation and the crystallization process when the MEAI portion is changed. Nevertheless, it can be seen that with increase of the MEA^+ portion resistance of the samples significantly increases. Irradiation of the films with the solar radiation simulator results in an increase of photocurrent approximately by two orders of magnitude.

The films of the hybrid perovskites are characterized by presence of ion migration at the room temperature, which results in degradation of the photovoltaic elements even under conditions of an inert atmosphere and with encapsulation of the devices. In the dark conditions, ion conductivity prevails at the room temperature [28]. Calculations using the density functional method show that intrinsic defects for $MAPbI_3$ (V_I^+, MA_i^+, V_{MA}^-, I_i^-) have low diffusion barriers, but V_I^+ has a much lower energy of formation and determines the main contribution to ion conductivity [29]. The study [30] reports about prevalent migration of iodine ions by means of iodine vacancies (vacancy-related migration of iodine ions). Ion migration and IVC hysteresis, reduced no-load voltage and reduced lifetime of the charge carriers, which are induced thereby, will depend on structural defects [28,31,32]. Thus, when varying the composition of the cations in $MA_{1-x}FA_xPbI_3$, the energy of activation of ion conductivity and efficiency of the devices correlated with the density and the structure of defects inside grains [31]. It was shown for the films of the hybrid perovskite $MAPbI_3$ that the increase of the grain size of the polycrystalline films resulted in increase of the energy of activation of ion conductivity, while the highest energy of activation was achieved in case of a single crystal [32]. Ion migration is usually reduced by using passivating molecules of cross linkers, thereby resulting in an increase of the energy of activation of ion conductivity, a decrease of hysteresis and an increase of longevity of the devices [28,33]. Probably, passivation of the grain boundaries results not only to reduction of the concentration of initial active defects on the grain boundary, but it also reduced mobility of the ions.

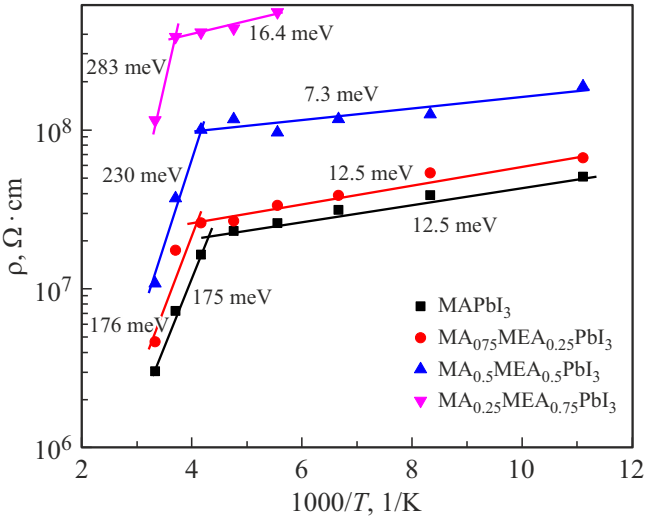


Figure 4. Temperature dependence of resistivity of the $MA_xMEA_{1-x}PbI_3$ films.

For the $MA_xMEA_{1-x}PbI_3$ films, ohmic portions of the I-V characteristics measured in darkness at the various temperatures shown in Figure 3 were taken to calculate the temperature dependences of resistivity, $\rho(T)$, which are shown in Figure 4. As follows from Figure 4, the dependences $\rho(T)$ for the studied samples have a complex activation nature and consist of two portions that can be described by the following expression:

$$\rho(T) = \rho_0 \exp\left(\frac{E_a}{k_B T}\right), \tag{1}$$

where E_a — the energy of activation, T — the temperature, k_B — the Boltzmann constant. The energies of activation were calculated from the temperature dependence of resistivity $\rho(T)$ by the formula:

$$E_a\,(\text{meV}) = \frac{200\Delta \lg(\rho)}{1000/T}, \tag{2}$$

where ρ — resistivity of the film; T — the temperature, 200 — the numerical coefficient (the value of $1/k_B$ in meV

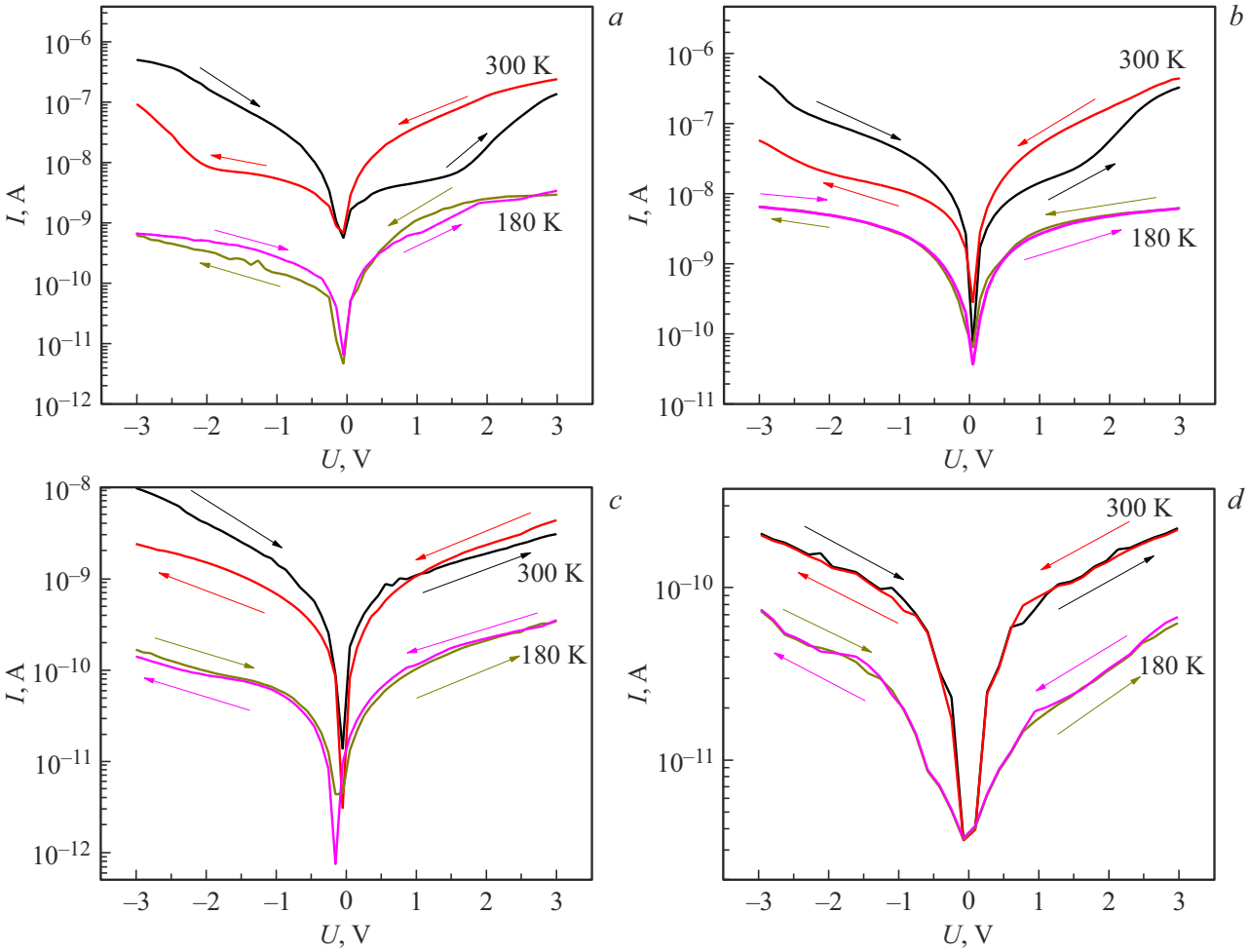


Figure 5. I-V characteristics of the $MA_xMEA_{1-x}PbI_3$ films at the temperatures 300 and 180 K. *a* — $x = 0$; *b* — $x = 0.25$; *c* — $x = 0.5$; *d* — $x = 0.75$.

that is multiplied to a coefficient when transiting into the respective coordinates $\lg\rho = f(1000/T)$).

As can be seen in Figure 4, the energy of activation of conductivity has two typical portions, which are related to electron conductivity at the low temperatures and ion conductivity at an increasing temperature. The energy of activation of electron conductivity is $\sim 10-20$ meV, which are typical values for the films of the hybrid perovskites [31]. With the increase of the MEA^+ portion, the energy of activation of ion conductivity increases (from 175 meV for $MAPbI_3$ to 283 meV for $MA_{0.25}MEA_{0.75}PbI_3$). A threshold temperature, at which ion conductivity starts prevailing is also shifted from 260 to 240 K. The increase of the energy of activation of ion conductivity correlates with the decrease of hysteresis of the I-V characteristics shown in Figure 5.

For the $MAPbI_3$ films, there is the largest IVC hysteresis at the room temperature, which decreases as MEA^+ increases, while for $MA_{0.25}MEA_{0.75}PbI_3$ no hysteresis induced by ion migration is observed. As can be seen from the I-V characteristics, no hysteresis except for slight IVC hysteresis for $MAPbI_3$is observed at the temperature of 180 K, which is below the temperature, when ion conductivity prevails. It is important to note that the hybrid perovskite $MA_{0.5}MEA_{0.5}PbI_3$ is attractive for use in the tandem solar cells with c-Si not only due to a suitable band gap, but because of reduced ion migration without additional passivation of the grain boundaries, too.

As mentioned above, the energy of activation of ion conductivity depends on the grain sizes, i. e. the defect density at the grain boundary, which provides the increase of ion migration. It was found in our previous studies that in these conditions of formation of the polycrystalline $MA_xMEA_{1-x}PbI_3$ films the increase of the MEAI portion in the solution results in a decrease of the grain sizes. Thus, the hysteresis reduction and the increase of the energy of activation of ion conductivity are related to a crystalline structure of $MA_xMEA_{1-x}PbI_3$ rather than to morphological specific features of the films. At the same time, disruptions of periodicity of the PbI_6 octahedrons (in the models with channels of the crystalline structure) with inclusion of MEA^+ complicate migration of the ions or increase the energy of their formation similar to use of cross linkers. Another mechanism of reduction of migration of the ions (in case of incorporation of MEA^+ into the crystalline structure without formation of the channels) may be interaction of the intrinsic defects V_I^+ and I_i^-

4. Conclusion

The study has investigated the influence of incorporation of the monoethanolammonium cations in the composition of the hybrid perovskite $MAPbI_3$ on the temperature dependences of the I-V characteristics and the energies of activation of ion conductivity. It was found that the increase of the portion of the monoethanolammonium cation in $MA_xMEA_{1-x}PbI_3$ resulted in the increase of the energy of activation, which was also accompanied by reduction of IVC hysteresis at the room temperature. The Fourier transform infrared spectroscopy showed appearance of the new intense peak with the significant increase of the MEA portion, which can be associated with OH groups and formation of the hydrogen bonds. The increase of the MEA portion also resulted in shifting of the band of N-H stretching, reduction of the peaks of CH_3 bending and CH_3NH_3 rocking, which are typical for pure $MAPbI_3$, as well as to appearance of a small absorption peak associated with CH_2 bending, which indicates chemical interaction of MEA in the composition of $MA_xMEA_{1-x}PbI_3$. It is shown than the increase of the MEA portion results in the increase of the energy of the absorption edge of the perovskite and the substantial change of the spectra shape as well as in the change of the energy band diagram. All the films of the hybrid perovskites demonstrate the photoresponse to irradiation in the visible spectral area, which is promising for use in the optoelectronic devices. In particular, the hybrid perovskites with the enlarged band gap are promising for use in the tandem solar cells. At the same time, the detected increase of the energy of activation of ion conductivity and reduction of IVC hysteresis at the room temperature contributes to reduction of degradation of the perovskite films included in the optoelectronic devices.

Acknowledgments

Regarding the synthesis of organometallic perovskites, the study was supported by a grant from the Republic of Belarus Foundation for Basic Research No. F23RNF-160 and the Russian Science Foundation No. 23-42-10029 (https://rscf.ru/project/23-42-10029/), dated December 20, 2022.

Conflict of interest

The authors declare that they have no conflict of interest.

References

[1] S. Khatoon, V. Chakravorty, J. Singh, R.B. Singh, M.S. Hasnain, S.M.M. Hasnain. Materials Science for Energy Technologies, **6**, 437–459 (2023). https://doi.org/10.1016/j.mset.2023.04.007.
[2] F. Khan, B.D. Rezgui, M.T. Khan, F.A. Al-Sulaiman. Renewable and Sustainable Energy Reviews, **165**, 112553 (2022). https://doi.org/10.1016/j.rser.2022.112553.
[3] X. Zhang, M.E. Turiansky, J.-X. Shen, C.G.V. d. Walle. Journal of Applied Physics, **131**, 9 (2022). https://doi.org/10.1063/5.0083686.
[4] B.G. Krishna, D.S. Ghosh, S. Tiwari. Solar Energy, **224**, 1369–1395 (2021). https://doi.org/10.1016/j.solener.2021.07.002.
[5] M. Ahmadi, T. Wu, B. Hu. Advanced Materials, **29**, 41 (2017). https://doi.org/10.1002/adma.201605242.
[6] Y. C. Kim, K.H. Kim, D.-Y. Son, D.-N. Jeong, J.-Y. Seo, Y.S. Choi, I.T. Han, S.Y. Lee, N.-G. Park. Nature, **550**, *7674*, 87–91 (2017). https://doi.org/10.1038/nature24032.

[7] X. Zhao, H. Xu, Z. Wang, Y. Lin, Y. Liu. InfoMat, **1**, *2*, 183–210 (2019). https://doi.org/10.1002/inf2.12012.
[8] X. Fan. Materials Today Sustainability, **24**, 100603 (2023). https://doi.org/10.1016/j.mtsust.2023.100603.
[9] B. Zhang, Y.-j. Liao, L. Tong, Y. Yang, X. Wang. Physical Chemistry Chemical Physics, **22**, *15*, 7778–7786 (2020). https://doi.org/10.1039/d0cp00866d.
[10] T. Zhu, M.-X. Li, C. Zhang, Y. Dong, F. Sun, D. Li, F. You, Z. He, C. Liang. Materials Today Chemistry, **39**, 102167 (2024). https://doi.org/10.1016/j.mtchem.2024.102167.
[11] Z. Shen, Q. Han, X. Luo, Y. Shen, Y. Wang, Y. Yuan, Y. Zhang, Y. Yang, L. Han. Nature Photonics, **18**, *5*, 450–457 (2024). https://doi.org/10.1038/s41566-024-01383-5.
[12] W. Feng, Y. Tan, M. Yang, Y. Jiang, B.-X. Lei, L.P. Wang, W.-Q. Wu. Chem, **8**, 351–383 (2022). https://doi.org/10.1016/j.chempr.2021.11.010.
[13] R. Azmi, E. Ugur, A. Seitkhan, F. Aljamaan, A.S. Subbiah, J. Liu, G.T. Harrison, M.I. Nugraha, M.K. Eswaran, M. Babics et al. Science, **376**, 73–77 (2022). https://doi.org/10.1126/science.abm5784
[14] T.L. Leung, I. Ahmad, A.A. Syed, A.M.C. Ng, J. Popović, W. Chen. Communications Materials, **3**, 63 (2022). https://doi.org/10.1038/s43246-022-00285-9.
[15] N. Mercier, S. Poiroux, A. Riou, P. Batail. Inorganic Chemistry, **43**, *26*, 8361–8366 (2004). https://doi.org/10.1021/ic048814u
[16] B. Cheng, T.-Y. Li, P. Maity, P.-C. Wei, D. Nordlund, K.-T. Ho, D.-H. Lien, C.-H. Lin, R.-Z. Liang, X. Miao, O.F. Mohammed, J.-H. He. Communications Physics, **1**, 1 (2018). https://doi.org/10.1038/s42005-018-0082-8
[17] A. Leblanc, N. Mercier, M. Allain, J. Dittmer, V. Fernandez, T. Pauporté. Angewandte Chemie International Edition, **56**, *50*, 16067–16072 (2017). https://doi.org/10.1002/anie.201710021
[18] C.C. Tsai, Y.-P. Lin, M.K. Pola, S. Narra, E. Jokar, Y.-W. Yang, E.W.-G. Diau. ACS Energy Letters, **3**, 2077–2085 (2018). https://doi.org/10.1021/acsenergylett.8b01046
[19] A. Ryabko, M. Ovezov, A. Tuchkovsky, O. Korepanov, A. Maximov, A. Komolov, E. Lazneva, E. Muratova, I. Vrublevsky, A. Aleshin et al. Nanomaterials, **15**, 494 (2025). https://doi.org/10.3390/nano15070494
[20] A. Rajagopal, K. Yao, A.K.-Y. Jen. Advanced Materials, **30**, 1800455 (2018). https://doi.org/10.1002/adma.201800455.
[21] G. Grancini, C. Roldán-Carmona, I. Zimmermann, E. Mosconi, X. Lee, D. Martineau, S. Narbey, F. Oswald, F.D. Angelis, M. Grätzel et al. Nature Communications, **8**, 15684 (2017). https://doi.org/10.1038/ncomms15684.
[22] M. García-Batlle, S. Deumel, J.E. Huerdler, S.F. Tedde, O. Almora, G. Garcia-Belmonte. Advanced Photonics Research, **3**, 12 (2022). https://doi.org/10.1002/adpr.202200136.
[23] M.A. Pérez-Osorio, R.L. Milot, M.R. Filip, J.B. Patel, L.M. Herz, M.B. Johnston, F. Giustino. The Journal of Physical Chemistry C, **119**, *46*, 25703–25718 (2015). https://doi.org/10.1021/acs.jpcc.5b07432.
[24] J. Sun, B. An, K. Zhang, M. Xu, Z. Wu, C. Ma, W. Li, S. Liu. Journal of Materials Chemistry A, **9**, *43*, 24650–24660 (2021). https://doi.org/10.1039/d1ta07498a.
[25] P. Jackson, K. Robinson, G. Puxty, M.I. Attalla. Energy Procedia, **1**, *1*, 985–994 (2009). https://doi.org/10.1016/j.egypro.2009.01.131.
[26] S.A. Legkov, G.N. Bondarenko, J.V. Kostina, E.G. Novitsky, S.D. Bazhenov, A.V. Volkov, V.V. Volkov. Molecules, **28**, 403 (2023). https://doi.org/10.3390/molecules28010403
[27] A.M.A. Leguy, P. Azarhoosh, M.I. Alonso, M. Campoy-Quiles, O.J. Weber, J. Yao, D. Bryant, M.T. Weller, J. Nelson, A. Walsh, M.V. Schilfgaarde, P.R.F. Barnes. Nanoscale, **8**, 6317–6327 (2016). https://doi.org/10.1039/c5nr05435d.
[28] X. Li, W. Zhang, Y.-C. Wang, W. Zhang, H.-Q. Wang, J. Fang. Nature Communications, **9**, 1 (2018). https://doi.org/10.1038/s41467-018-06204-2.
[29] D. Yang, W. Ming, H. Shi, L. Zhang, M.-H. Du. Chemistry of Materials, **28**, *12*, 4349–4357 (2016). https://doi.org/10.1021/acs.chemmater.6b01348.
[30] C. Eames, J.M. Frost, P.R.F. Barnes, B.C. O'Regan, A. Walsh, M.S. Islam. Nature Communications, **6**, 1 (2015). https://doi.org/10.1038/ncomms8497.
[31] W. Li, M.U. Rothmann, Y. Zhu, W. Chen, C. Yang, Y. Yuan, Y.Y. Choo, X. Wen, Y.-B. Cheng, U. Bach. Nature Energy, **6**, *6*, 624–632 (2021). https://doi.org/10.1038/s41560-021-00830-9.
[32] J. Xing, Q. Wang, Q. Dong, Y. Yuan, Y. Fang, J. Huang. Physical Chemistry Chemical Physics, **18**, *44*, 30484–30490 (2016). https://doi.org/10.1039/c6cp06496e.
[33] B. Han, S. Yuan, B. Cai, J. Song, W. Liu, F. Zhang, T. Fang, C. Wei, H. Zeng. Advanced Functional Materials, **31**, 26 (2021). https://doi.org/10.1002/adfm.202011003.

Translated by M.Shevelev